Water absorption and chloride diffusivity of concrete under the coupling effect of uniaxial compressive load and freeze-thaw cycles

Yanru Wang [a, b], Yubin Cao [a, b], Peng Zhang [a, *], Yuwei Ma [d, b, *], Tiejun Zhao [a], Hao Wang [b], Zuhua Zhang [b, c]

[a] *College of Civil Engineering, Qingdao University of Technology, Qingdao, 266033, PR China*
[b] *Centre for Future Materials, University of Southern Queensland, Toowoomba, QLD 4350, Australia*
[c] *Key Laboratory for Green & Advanced Civil Engineering Materials and Application Technology of Hunan Province, College of Civil Engineering, Hunan University, Changsha 410082, PR China*
[d] *Guangzhou University - Tamkang University Joint Research Center for Engineering Structure Disaster Prevention and Control, Guangzhou University, Guangzhou 510006, China*

E-mails of corresponding authors: peng.zhang@qut.edu.cn; yuwei.ma@hotmail.com

Abstract:

In cold coastal area, the destruction mechanism of reinforced concrete structures is mainly governed by a combination of factors such as self-loading, freeze-thaw and chloride erosion. In this study, ordinary cube concretes (C30 and C50, while w/c = 0.53 and 0.35 respectively) underwent a coupling effect of pressure load with stress ratio of 0, 0.3 and 0.5 and freeze-thaw cycles, following by capillary water absorption test and chloride penetration test. Concrete samples with $0.3f_c$ showed the best water and chloride penetration resistance under the coupling effect, followed by samples with $0.5f_c$ and $0f_c$, which is consistent with the conclusion that under load only. Water and chloride ions penetration increased sharply when freeze-thaw cycles was over 100 times, which is different with samples without load. Outside part of concrete showed higher permeability and chloride content than inside part. MIP results confirmed that stress played an important role in the water absorption and chloride penetration

of concrete under the coupling effect. These results provide important new insights into the permeability of concrete under a coupling effect. The applied load performed a more important role on the service life prediction of concrete structure.

Keywords: Coupling effect; Freeze-thaw; Load; Capillary Water; Chloride

1. Introduction

Reinforced concrete is widely used in construction around the world, mainly due to its low cost, high mechanical strength and stability [1]. However, deterioration of concrete structures have been reported both in literature and in practice, particularly when concrete is served in harsh environment, leading to decline of concrete strength and corrosion of reinforced rebar [2, 3]. It is thus accepted that the durability and service life of concrete structures should be considered in future construction design. In general, the durability and service life of concrete are mainly governed by a series of environmental factors, e.g. freeze-thaw, carbonation, sulphate attack and chloride penetration etc. [4]. In practice, most concrete structures are exposed to coupling environmental actions. In cold coastal area, such as the north area of China, freeze-thaw and chloride penetration are the main deteriorating processes for reinforced concrete structures [5].

Chloride ions were detrimental ions affecting the service life of reinforced concretes. The presence of free chloride ions in environments could penetrate concrete and result in corrosion of reinforced bar. According toYang et al. [6], the main transport processes in concrete included capillary absorption, diffusion, permeation, and convection. As for capillary force or gradient of capillary potential, the water is absorbed into concrete through pores, while diffusion

happened mainly because of a concentration gradient [7, 8]. Penetration is a transport process of water and air into concrete, which is caused by gravity or pressure gradient; and convection is the process happened in solution such as the transport of chloride or sulphate ions into concrete [9, 10]. In real construction, it is usually more than one process occurring at the same time, and each of these mechanisms are influenced by internal microstructure of concrete and external environment.

The pore structure of concrete has a crucial influence on the process of chloride penetration; and water is the main transfer medium [11-18]. According to Mehta [19] and Chen [20], with the decrease of the pore aperture size (r), the water penetration depth decreases firstly ($r \geqslant$ 1000 ~ 10000 nm) and then increase (100 nm $\leqslant r \leqslant$ 1000 nm), and finally decreased again ($r \leqslant$ 100 nm). In addition, the aperture size smaller, the freezing point lower, and the freezing rate in concrete pore lower. Finally, the damage caused by the expansion of pore water lower [21].

Hence, study on the migration of water in concrete is important. The frozen of pore solution caused by freeze-thaw process created internal pressure in pores and led to damage of concrete. The respective effect of chloride penetration and freeze-thaw cycles on the durability of concrete has been extensively investigated in previous studies [22-25]. It was reported that the penetration of chloride into concrete was related to the pore structure and cracks in concrete [23, 26-28]. Costa and Appleton [29] presented the results of an experimental study of the two concrete mixes (water/cement ratio = 0.3 and 0.5) in four different marine exposure conditions

(spray zone, tidal zone, atmospheric zone and dockyard zone) for five years. The results showed that the chloride penetration of concrete (w/c = 0.5) in tidal zone was highest. The authors speculated that the chloride penetration strongly dependent on both the concrete mixture and the exposure conditions. Collepardi et al. [30] did chloride diffusion test of Portland cement at different experimental temperature, i.e. 10°C, 20°C and 40°C and found that the diffusion coefficients of chloride ion into Portland cement pastes increased with the increase of temperature.

Freeze-thaw cycles accelerate the damage evolution of concrete and reduce the service life of concrete structures. Cai and Liu [31] observed the change of electrical conductivity of concrete exposed to a refrigerator (temperature varied from 0 °C to -20 °C) and concluded that the frozen of pore solution between 0 °C to -10 °C determined the durability of concrete. Molero et al. [32] applied ultrasonic imaging to evaluation the degradation process of normal concrete and air-contained concrete exposed to freeze-thaw cycles and found that the later showed better frost resistance than the former.

Studies also suggested that the main factor to improve the freeze-thaw resistance relied on the compact of concrete . explained that mix design of concrete could influence its compaction energy, which then significantly affected the freeze-thaw durability of Portland cement concrete and, to a less extent, reduced compressive strength and split strength and increased permeability.

Apart from single environmental factor, coupling effect of two or more environmental factors is considered recently. Zhang et al. [23] used Neutron radiography to study the influence of freeze-thaw cycles on capillary absorption and chloride penetration concrete. They found that the freeze-thaw cycles increased the rate of water absorption and chloride penetration. Yang et al. [6] studied water transport in concrete after freeze-thaw cycling. They found that both the total water absorption and the initial water absorption coefficient increased after 500 freeze-thaw cycles due to the frost induced cracks.

In practise, most reinforced concrete structures are used under load. The consideration of load combined with environmental actions could provide more practical and reliable results when evaluate the durability and service life of concrete. Sun and Lu [33] demonstrated that the permeability of concrete increased under 60% ultimate load during coupling effect of axially distributed load and carbonization. Bao and Wang [34] found that with the increase of compression stress load, the chloride content decreased firstly and then increased after a critical stress level. Sun et al. [35] found that the stress ratio was an important influencing factor on performance of concrete; concrete subjected to higher stress ratio, presented greater frost damage.

The previous study most focus on mechanical load and one environmental load (i.e. load + carbonization/freeze-thaw/chloride penetration et al.) or two environmental loads (i.e. freeze-thaw + carbonization/chloride penetration). This paper studied the coupling effect of mechanical load and two environmental loads, i.e. mechanical load + freeze-thaw + chloride

103 penetration, which could provide a new insight on the prediction of reinforcement concrete
104 structure.

105 2. Materials and Methods

106 2.1 Materials

107 Portland cement Type I was used as the raw material for the concrete. The chemical
108 composition of cement measured by X fluorescent spectrometry (XRF) was shown in Table 1.
109 Its specific surface area was 350~370 m^2/kg. The average particle size was around 27 μm; and
110 the particles size less than 3 μm and 3-30 μm accounted for about 6.7% and 70%, respectively,
111 meeting the requirements for optimum cement performance proposed by Tsivilis et al. [36].
112 River sand with a Fineness modulus of 2.7 and granite gravel with a distribution diameter
113 between 5 mm and 20 mm (obtained from Qingdao, China) were used as fine aggregate and
114 coarse aggregate, respectively. For C50 concrete, PCA®-I polycarboxylic acid high
115 performance water reducing agent (produced by Subute New Materials Co., Ltd.) were used to
116 obtain the slump and fluidity in line with real construction requirements.

117 2.2 Sample preparation

118 Concrete was prepared with by different strength category, i.e. C30 and C50, according to
119 JGJ/55-2011 [36]. Table 2 shows the mixture composition of each concrete. The water to
120 cement ratio for C30 and C50 was 0.53 and 0.35, respectively. Firstly, mixing solid materials
121 at horizontal concrete mixer for 1 minute, then add water (with superplastizer) into mixture

stirring for another 3 minutes. After mixing, fresh concrete was cast into 100 mm ×100 mm × 100 mm cube mould. After 1 day curing at room temperature, all concrete specimens were demoulded and cured in a curing room (relative humidity of 95% and temperature of 20 ± 2 °C) for 23 days. Before loading and freeze-thaw test, concrete samples were immersed into water for another 4 days until saturated.

2.3 Experimental methods

2.3.1 Loading and freeze-thaw tests

At 28 days, the compressive strength (f_c) of C30 and C50 were measured according to GB/T 50081-2002 [37], and the results were shown in Table 3. In loading test, hydraulic jack was used to supply stress on specimen. Two different compression stress level, i.e. $0.3f_c$ and $0.5f_c$ were applied on. The exact pressure applied on concrete specimens can be read from a dial attached to the hydraulic jack. Hydraulic pressure testing machine which was usually used by normal compression test was also used in this study for comparison [38]. It was found that the deviation of compressive strength results measured by hydraulic jack and hydraulic pressure testing machine was less than 2 MPa. During the loading process, the whole loading devices (including concrete specimens) were immersed in water for 4 days and then exposed to freezing-thawing test according to GB/T 50082-2009 [39]. Every freeze-thaw cycle continued for 3.5 h, with the highest temperature of 18±2 °C and lowest temperature of -20±2 °C. In total, 150 freezing-thawing cycles were conducted. The sequences of test flow were compiled in Fig. 1.

2.3.2 Mass-loss testing

The mass loss reflected the frost resistance of concrete. In this study, the mass loss of C30 and C50 concrete without load was measured by electronic scale (with an accuracy of 0.05 g) during freeze-thaw test. The average mass loss of three concrete specimens was used as the final value.

2.3.3 Relative dynamic elasticity modulus characterization

Frost damage could influence the pore structure of concrete which could be reflect by its relative dynamic elasticity modulus (RDM). The machine used for RDM test in this contribution is KON-NM-4B non-metal ultrasonic testing analyser (CX2009XJ0179, Koncrete, China), which includes transmitting port (output high voltage pulse) and receiving port (receiving ultrasonic waves through concrete). After freeze-thaw cycles, the change of cracks and pore structure inside concrete affected the transportation of ultrasonic waves through concrete, directly reflected in the transport velocity values (V_n). Relative dynamic modulus (E_{rd}) was calculated by Eq. (1). According to ACTM C 666 [32, 40], concrete was damaged once its RDM loss exceed the critical value (i.e. 60%).

$$E_{rd} = \frac{E_{dn}}{E_{d0}} = \frac{{V_n}^2}{{V_0}^2} \quad (1)$$

Where, E_{rd} = the relative dynamic modulus, %;

E_{dn} = the dynamic modulus of concrete after n freeze-thaw cycles, Hz;

E_{d0} = the dynamic modulus of concrete before freeze-thaw cycles, Hz;

159 V_n = the transport velocity values after n freeze-thaw cycles, m/s;

160 V_0 = the transport velocity values before freeze-thaw cycles, m/s;

161 **2.3.4 Capillary water absorption test and Chloride penetration test**

162 **2.3.4.1 Cutting**

163 After certain freezing-thawing cycles (0, 25, 50, 100 and 150 cycles), the concrete specimens
164 were unloaded and cut into four pieces. One cube concrete specimen were divided into two
165 sets; each set includes one inside piece and one outside piece. One set was used for capillary
166 water absorption test and the other one was used for chloride penetration test. Table 4 shows
167 the definition examples of different concrete specimens. Specimens were designate in the form
168 of "XX-CC-i/o" where XX representing applied compression stress level, CC representing
169 frost cycles, and i/o representing inside piece or outside piece of concrete specimen. After
170 cutting, all pieces were dried in oven at 60 °C for 24 h and then cooled to ambient temperature
171 for 12 h. This step could evaporate all free water inside of concrete to improve the accuracy of
172 the water absorption tests and chloride intrusion [41]. To ensure one-dimensional diffusion of
173 moisture, the other four sides of concrete piece that are perpendicular to the absorbent surface
174 were sealed with paraffin wax [42].

175 **2.3.4.2 Water absorption test**

176 When concrete was exposed to water, water could enter inside of materials through capillary
177 pressure. This phenomenon was related to many durability related issues, e.g. chloride

penetration, hence damage the concrete structure [38, 43, 44]. The water absorption of concrete were measured by the time dependent amount of water that was absorbed by capillary pores in concrete. The amount of capillary absorption water of concrete gradually decays with the square root of absorption time, which could be described using the following equation [23, 43].

$$\Delta W = A\sqrt{t} \tag{2}$$

Where, A = the water absorption coefficient, g/m^2·h$^{0.5}$; t = the immersion time of specimens in water or 3.5% NaCl solution, hour; t varies from 0 h, 0.5 h, 1 h, 2 h, 4 h, 8 h, 12 h, 24 h, 48 h, 72 h, 168 h, 336 h and 672 h.

Due to the effect of gravity, the mass of absorbed water could compensate with capillary pressure with the increase of absorbed time. As shown in Fig. *4* and Fig. *5*, the lines tend to steady with the increase of time. This process could be described in an empirical exponential function as shown in Eq. (3). The parameters a and b was determined by fitting Eq. (2) with experimental data as shown in Fig. *4* and Fig. *5*.

$$\Delta W = a\left[1 - \exp(-b\sqrt{t})\right] \tag{3}$$

The time-dependent coefficient ($A(t)$) of capillary water absorption was obtained by Eq. (4). The initial coefficient of capillary water absorption A_i could be determined by Eq. (5) [23, 38].

$$A(t) = \frac{d\Delta W}{d\sqrt{t}} = a \times bexp(-b\sqrt{t}) \tag{4}$$

$$A_i = a \times b \tag{5}$$

2.3.4.3 Chloride Penetration tests

1) Preparation of concrete powder

As mentioned in Section 2.2.3.1, one outside concrete piece and inside concrete piece were put in contact with NaCl solution with a concentration of 3.5%. The experiment set-up is the same as the water absorption test. After exposure to NaCl solution for certain age (7 days and 28 days), concrete were taken out of the container and grinded into powder layer by layer [45]. For the grinding procedure, the concrete block was first fixed on the grinding machine, and the grinding head was adjusted to contact the surface of concrete and started to grind. The grinding machine was shown in [45]. Each layer was milled with a thickness of 2 mm. In total, a depth of 20 mm was ground for each concrete specimen. The obtained concrete powder was sieve with a 0.63 mm sieve-mesh and dried in an oven at a temperature of 55 ± 5 °C for 2 hours. After drying, concrete powder was put in in a desiccator to room temperature, and then sealed for use.

2) Determination of chloride ion content

The chloride content of the obtained powder was determined according to GB11896-89 [46]. In this experiment, 2 grams of concrete powder was mixed with 50 ml distilled water (V_1) and shake for 15-20 minutes. After mixing the suspension liquid was stand still for 24 hours and filtered. Afterwards, 20 ml filtrate (V_2) was pipetted and put into an Erlenmeyer flask. 2 drops of phenolphthalein was first added in the solution, then neutralized with dilute sulfuric acid until the solution became colourless. Afterwards, 10 drops of potassium chromate reagent was

added in the flask, and titrated with standard silver nitrate solution (0.02 mol/L) to become red colour and recorded the volume (V_3) consumed by silver nitrate.

The free chloride content was calculated as Eq. (6) [47, 48]:

$$P = \frac{C_{AgNO_3} V_3 \times 0.03545}{G \times \frac{V_2}{V_1}} \times 100\% \quad (6)$$

Where: P = the free chloride content in concrete;

G = the weight of concrete powder, 2 grams;

V_1 = the water used to dissolved concrete powder, 50 ml;

V_2 = the filtrate used for titration, 20 ml;

V_3 = the $AgNO_3$ used for titration.

2.3.5 Mercury intrusion porosimetry test (MIP)

The mercury intrusion porosimetry used in this study is Pore – master – 33. The measurement was conducted in two stages: the first stage is the low pressure stage; the second stage is the high pressure stage. The highest pressure can reach 33000 Psi (1 Psi = 6.895 kPa). Washburn equation (Eq. (6)) was used to calculate the diameter of pores intruded by mercury at each pressure step.

$$D = -4\gamma cos\theta / P \quad (6)$$

Where D is the pore diameter, γ is the surface tension of mercury, θ is the contact angle between mercury and AAF materials and P is the applied pressure. The surface tension used here is 0.485 N/m, and the contact angle is 132°. According to Washburn equation, the pore size ranging from 360 μm to 0.005 μm can be detected in this study.

The samples used for MIP test were damaged concrete pieces that was exposed to frost cycles and applied load. First, concrete piece was broken by hammer with hand and coarse aggregate were removed out from mortar. The mortar was then immediately immerged in ethanol to terminate the hydration. Before test, samples were dried by oven and cooled to room temperature.

3. Results and discussion

3.1 Mechanical behaviour

3.1.1 The mass loss of concrete exposed to freeze-thaw cycles

Fig. *2* shows the mass loss rate of C30 and C50 concrete during freeze-thaw cycles without loading. For C30 concrete, there is a sharp mass-loss after 25 frost cycles which indicating the initiation damage of concrete. C50 concrete showed much slower weight loss than C30 concrete during frost cycles. For example, when freeze-thaw cycles reached 150 times, the mass loss rate of C50 was 0.59%, significantly lower than that of C30 concrete (4.49%). The mass loss of concrete was mainly caused by the loss of mortar on the concrete surface [49]. C50 concrete had lower water/cement ratio and denser microstructure than C30 concrete.

Hence during freeze-thaw cycles, the saturated water in C50 concrete was lower than C30 concrete, resulting in less damage during frost cycles. Water/cement ratio showed importance in frost resistance of ordinary Portland concrete [50].

3.1.2 The loss of relative dynamic modulus (RDM) of concrete under compressive load and freeze-thaw cycles

Fig. 3 shows the change of RDMs of C30 and C50 concrete under different compression stress ratio and frost cycles. It is obvious that the RDMs of C30 and C50 both decreased with increasing frost cycles. It is interesting to find that concrete samples under 30%ultimate load ($0.3f_c$) presented the smallest RDM loss than samples without loading ($0f_c$) and with 50% ultimate load ($0.5f_c$). For example, the RDM loss of C30 concrete with $0.3f_c$ load was 7.9%, compared to 39.4% and 43.1% for concrete C30 with $0f_c$ load and $0.5f_c$ load, respectively. The same phenomenon was also found in C50 concrete. It means that the application of a certain compressive load on concrete could increase its frost resistance. Compared to C30 concrete, C50 concrete had less RDM loss after same freeze-thaw cycles, which means C50 concrete performed better frost resistance than C30 concrete.

It is speculated that the loss process of RDM depended on the pore structure in concrete during the freeze-thaw process. At low temperature (lower than 0°C), the volume of closed pore in concrete expanded due to icing [51]. This expand force was counteracted by a certain compressive load. Thus, when the compressive ratio was 0.3 ($0.3f_c$), concretes showed higher frost resistance than concretes without loading. With the increase of loading (stress ratio is 0.5

in this study), the applied stress exceeded the expand force, secondary cracks were generated [52-54]. As discussed in section 2.3.3, cracks inside concrete reduced the transport velocity values, which leading to a higher RDM loss.

3.2 Water absorption of concrete under coupling effect of compressive load and freeze-thaw cycles

Water absorption was regarded as a useful indicator to evaluate the damage of concrete under coupling effect of compressive load and freeze-thaw cycles [41]. Fig. 4 shows the amount of absorbed water of C30 concrete under coupling effect of load and freeze-thawing cycles. It was found that the amount of absorbed water increased with the immersing time. For outside concrete specimens, the amount of absorbed water of concrete under 30% ultimate load ($0.3f_c$) shows lower water absorption content than that without load, while the concrete under 50% ultimate load ($0.5f_c$) shows the highest. For inside concrete specimens, it is clear to see that the concrete under $0.5f_c$ shows relatively higher water absorption amount, while concrete under $0.3f_c$ shows similar water absorption amount in comparison with that without load.

As shown in Fig. 4, the black dashed line is the base line of samples without any damage from frost and load. Compare spacing between the black dashed line with samples, we could find that the increment of the amount of absorbed water of the samples under $0.3f_c$ is smaller than other two samples. Particularly, when frost cycles increased from 25 to 50, there is inconspicuous increase for samples under $0.3f_c$. It is different with the results that observed by Zhang et al. [23], the amount of absorbed water increased with freeze-thaw cycles (0, 10, 50

and 100 cycles) if samples without applied load. This means that the service life prediction of concrete structures becomes complex if applied mechanical load and environmental load.

It is known that water absorption content was closely related to the capillary pores in concrete. A certain compressive stress could compact existing cracks in concrete and hinder the generation of new cracks, resulting in a lower water absorption content. When the applied load reached 50% ultimate load ($0.5f_c$), the excessive load induced new cracks in concrete and then water absorption content increased. Bao and Wang [34] also found that cumulative water content decreased when applied load increased from 0% to 19.81%, and then increased from 34.21% to 49.55%. We could find that, the influence of applied load on water absorption of concrete showed less difference with or without freeze-thaw cycles.

The amount of absorbed water increased when frost cycles increased from 50 to 150. It indicates that the frost damage generated more cracks in concrete with the increase of freeze-thaw cycles. The new cracks provided more penetration path for water into concrete.

The amount of absorbed water of inside concrete specimen was less than that of the outside specimens. It means that the damage caused by freeze-thaw cycles initiated from the outside, then developed to the inside part [23]. It is reported that the freeze-thaw damage on concrete included two aspects [6]: first is the peeling off surface mortar and then generation of internal cracks. In this study, it is found that the internal damage happened after 50 freeze-thaw cycles, before which the water absorption content was similar to inside samples (Fig. 4).

Fig. 5 shows the amount of absorbed water of C50 concrete under the coupling effect of load and freeze-thaw cycles. In general, the amount of absorbed water of C50 exhibited similar trend as C30, while the water absorption content of C50 was about 5 times smaller than that of C30, both before and after the freeze-thaw cycles. It means that C50 concrete have a better water resistance than C30 concrete under the coupling effect of load and frost cycles.

It is interesting to note that the water absorption content of C50 concrete under 30% ultimate load ($0.3f_c$) showed close trend to that without loading. Samples under 50% ultimate load ($0.5f_c$) showed a little higher water absorption content. Compared with C30 concrete, samples under 50% ultimate load (0.5fc) showed a significant increase than that without loading. It means that the applied stress had less influence on low water/cement ratio concrete (i.e. C50, w/c=0.35) than high water/cement ratio concrete (i.e. C30, w/c=0.53).

Fig. 6 summarized the initial water absorption coefficient (A_i) of C30 and C50 as a function of freeze-thaw cycles. It is clear that A_i exhibits an upward trend with the increase of freeze-thaw cycles. For C30 concrete, after 50 freeze-thaw cycles, the A_i increased sharply. It means that new cracks generated in concrete after 50 freeze-thaw cycles. For C50 concrete, the A_i was much smaller than C30 concrete. The coupling effect of compressive load and freeze-thaw cycles was more serious on C30 concrete than on C50 concrete [50].

3.3 Chloride penetration of concrete under compressive load and freeze-thaw cycles

Fig. 7 and Fig. 8 show the chloride ion content of C30 concrete after 7d and 28 d chloride penetration, respectively. The chloride ion content described with increasing depth. This is because that chloride ions penetrated into concrete surface by capillary suction and then diffused into deeper zones [38].

From Fig. 7, it is obvious that samples with $0.3f_c$ showed the least chloride ion content and samples with $0.5f_c$ showed the highest. It means that $0.3f_c$ could help hinder the penetration of chloride ion while $0.5f_c$ accelerate the penetration. This is because that a certain compression stress level compact the pore structure of concrete. The penetration of chloride ion into concrete was hindered [35, 38, 55, 56]. The penetration depth and the amount of chloride ion significantly increased with the increase of freeze-thaw cycles. Frost action before 50 freeze-thaw cycles did not apparently influence the penetration of chloride ion, which similar to the water absorption [57]. Compared with the results found by Zhang et al. [23], the amount of chloride pentation increased obviously with the increase of freeze-thaw cycles without load. The chloride penetration became complex and unstable if applied load. The results suggested that a certain compression load was encouraged for concrete structure in cold coast area [26]. It suggested that a certain of compressive stress should be concerned into the durability design of reinforcement concrete structure.

340 It is also found that the chloride ion content of inside concrete specimen was less than that of
341 the outside part. This is because that the peeling off of the surface of outside part which exposed
342 to freeze-thaw solution provided new penetration pathway for chloride ion into concrete [23,
343 58]. It is suggested that a protective treatment on the surface of concrete could develop to
344 enhance the durability of structure.

345 From the comparison of Fig. 7 and Fig. 8, it is obvious that the penetration depth and amount
346 of chloride ion increased significantly after 28 d chloride penetration. For example, the chloride
347 ion content of 7 d at 20 mm depth was less than 0.05% of concrete while chloride ion content
348 of 28 d still kept down trend after 20 mm. According to Wittmann et al. [59], raw material and
349 tap water could carry around 0.05% chloride into concrete. This means that in this study
350 chloride ion penetrated into deeper depth than 20mm after 28d penetration [23, 38].

351 Fig. 9 and Fig. 10showed the chloride ion content of C50 concrete after 7 d and 28 d chloride
352 penetration. Similar change trend of chloride ion content occurred between C30 and C50 refer
353 to the influence of coupling effect of freeze-thaw and stress level. It is noted that the chloride
354 ion content of C50 tended to smooth at 10 mm while C30 concrete kept downward trend after
355 20 mm. Chloride penetration rate of C50 was much lower than C30. This indicated that C50
356 performs better chloride resistance than C30. This observation can be explained
357 phenomenologically by the difference of water/ratio. Lower w/c ration could synthesis more
358 impact concrete and shows higher damage resistance to coupling effect [23, 50]. Wang et al.

[48] also found that with the increase of the compressive stress (from 22% to 51%), the chloride concentration at a given depth was decreased, especially for the concretes C30 (w/c = 0.50) .

3.4 Pore size distribution

Fig. 11 showed the pore size distribution of C30 concrete under different compressive stress ratio after 50 freeze-thaw cycles. For all the samples, generally one peak (in the range of 10-1000 nm) was shown in Fig.15, representing the capillary pores of C30. Due to "ink-bottle" effect and contact angle, the real pore diameter of capillary pores in C30 may be tens of times larger than the results in MIP. However, the comparison of equal treatment samples can still provide some valuable information on the pore structure.

As suggested by Mehta [19] and Chen [20], capillary effect decreased firstly and then increased with the pore size decreased from 10000nm to 100nm. After 50 freeze-thaw cycles, the peak corresponding to the capillary pore in $0.5f_c$ was the highest, while the peak of $0f_c$ (without loading) and $0.3f_c$ was lower, indicating that concrete samples under $0.5f_c$ was the highest water absorption and chloride induction. Samples without load or freeze-thaw cycles showed the smallest peak value and relatively lower amount of absorbed water and chloride ions.

From comparison between undamaged samples with damaged samples, it proves that frost action lead to a percentage increment of coarse pores, resulting in an increment of absorbed water and chloride. At the meantime, 50% ultimate compressive stress encouraged the frost damage while 30% ultimate compressive stress could reduce.

From above results, we could confirm that stress played a relatively important role in the water absorption and chloride penetration of concrete under coupling effect of load and freeze-thaw. It means that a certain stress level (30% ultimate strength in this study) could improve the resistance of concrete to water and aggressive solution during freeze-thaw cycles. The above result provided key information regarding to the service life design or durability design of concrete structure in cold coast area.

4. Conclusions

From the result presented in this paper, the following conclusions can be drawn:

1. The amount of absorbed water and chloride ion increased slightly before 50 freeze-thaw cycles and sharply after 100 and 150 cycles. Freeze thaw shifted the pore size distribution towards microporous and generate new cracks, which provided new penetration path for water and chloride ion into concrete.
2. C50 concrete showed better penetration resistance to water and chloride ion than C30 concrete. The effect of applied load had much less impact on the Cl penetration than C30 concrete. Water/cement ratio is the decisive factor on the durability performance of concrete. The applied load ($0.3f_c$) had inconspicuous effect on C50 concrete.
3. For C30 concrete, a certain stress ($0.3f_c$) could help relieve the damage caused by frost and Cl ingression, while excessive load ($0.5f_c$) could aggravate damage. The influence of load should be concerned into the durability design of reinforcement concrete structure exposed to marine environment.

4. Under coupling effect of load and freeze-thaw, applied load could cause significant change to the freeze-thaw resistance of concrete; however, the unfluence of load on the durability of concrete is slightly changed by freeze-thaw.

Acknowledgements

Financial support of ongoing projects by Natural Science Foundation of China (51420105015, U1706222, 51778309), 973 Program (2015CB655100), and Natural Science Foundation of Shandong Province (ZR201709210171, ZR2017ZC0737) is greatly acknowledged.

References

1. Aïtcin, P.-C., Cements of yesterday and today: Concrete of tomorrow. Cement and Concrete Research, 2000. **30**(9): p. 1349-1359.
2. Powers, T.C. A working hypothesis for further studies of frost resistance of concrete. in Journal Proceedings. 1945.
3. Wang, P.G., et al. Influence of Sustained Load on Durability and Service Life of Reinforced Concrete Structures. in Key Engineering Materials. 2016. Trans Tech Publ.
4. Glasser, F.P., J. Marchand, and E. Samson, Durability of concrete—degradation phenomena involving detrimental chemical reactions. Cement and Concrete Research, 2008. **38**(2): p. 226-246.
5. Pigeon, M. and R. Pleau, Durability of concrete in cold climates. 2010: CRC Press.
6. Yang, Z., W.J. Weiss, and J. Olek, Water Transport in Concrete Damaged by Tensile Loading and Freeze–Thaw Cycling. Journal of Materials in Civil Engineering, 2006. **18**(3): p. 424-434.
7. Wilson, M., M. Carter, and W. Hoff, British Standard and RILEM water absorption tests: A critical evaluation. Materials and Structures, 1999. **32**(8): p. 571-578.
8. Dullien, F.A., Porous media: fluid transport and pore structure. 2012: Academic press.
9. Boddy, A., et al., An overview and sensitivity study of a multimechanistic chloride transport model. Cement and concrete research, 1999. **29**(6): p. 827-837.
10. Yong, R.N., A.-M.O. Mohamed, and B.P. Warkentin, Principles of contaminant transport in soils. 1992: Elsevier Science Publishers.
11. Gutiérrez-Padilla, M.G.D., et al., Biogenic sulfuric acid attack on different types of commercially produced concrete sewer pipes. Cement and Concrete Research, 2010. **40**(2): p. 293-301.
12. Wang, L. and S. Li, Capillary absorption of concrete after mechanical loading. Magazine of Concrete Research, 2014. **66**(8): p. 420-431.
13. Martys, N.S. and C.F. Ferraris, Capillary transport in mortars and concrete. Cement and Concrete Research, 1997. **27**(5): p. 747-760.
14. Dehghanpoor Abyaneh, S., H.S. Wong, and N.R. Buenfeld, Computational investigation of capillary absorption in concrete using a three-dimensional mesoscale approach. Computational Materials Science, 2014. **87**: p. 54-64.
15. Mors, R.R.M.M.t.n.b.c. and H.H.M.J.t.n. Jonkers, Effect on Concrete Surface Water Absorption upon Addition of Lactate Derived Agent. Coatings (2079-6412), 2017. **7**(4): p. 1-10.
16. Soroushian, P., H. Chowdhury, and T. Ghebrab, Evaluation of Water-Repelling Additives for Use in Concrete-Based Sanitary Sewer Infrastructure. Journal of Infrastructure Systems, 2009. **15**(2): p. 106-110.
17. Şahmaran, M. and V.C. Li, Influence of microcracking on water absorption and sorptivity of ECC. Materials and Structures, 2009. **42**(5): p. 593-603.
18. Wu, L., et al., Autogenous shrinkage of high performance concrete: A review. Construction and Building Materials, 2017. **149**: p. 62-75.

19. Mehta, P.K., Studies on blended Portland cements containing Santorin earth. Cement and Concrete Research, 1981. **11**(4): p. 507-518.
20. Chen, L.W., Yongping; Yin, Xinshen; Zhang, Dan, Effect of aperture size on impermeability of concrete. Journal of The Chinese Ceramic Society, 2005. **33**(4): p. 500-505.
21. Zhang, S.P. and L. Zong, Evaluation of Relationship between Water Absorption and Durability of Concrete Materials. Advances in Materials Science & Engineering, 2014: p. 1-8.
22. Zuquan, J., et al., Chloride ions transportation behavior and binding capacity of concrete exposed to different marine corrosion zones. Construction and Building Materials, 2018. **177**: p. 170-183.
23. Zhang, P., et al., Influence of freeze-thaw cycles on capillary absorption and chloride penetration into concrete. Cement and Concrete Research, 2017. **100**: p. 60-67.
24. Cui, F.-k., et al., Mechanical and Failure Criteria of Air-Entrained Concrete under Triaxial Compression Load after Rapid Freeze-Thaw Cycles. Advances in Materials Science & Engineering, 2017: p. 1-8.
25. Zhang, P., et al., Effect of Air Entrainment on the Mechanical Properties, Chloride Migration, and Microstructure of Ordinary Concrete and Fly Ash Concrete. Journal of Materials in Civil Engineering, 2018. **30**(10): p. 04018265.
26. Zhang, P., et al., Steel reinforcement corrosion in concrete under combined actions: The role of freeze-thaw cycles, chloride ingress, and surface impregnation. Construction and Building Materials, 2017. **148**: p. 113-121.
27. Tennakoon, C., et al., Chloride ingress and steel corrosion in geopolymer concrete based on long term tests. Materials & Design, 2017. **116**: p. 287-299.
28. Zhang, P., et al., Application of neutron imaging to investigate fundamental aspects of durability of cement-based materials: A review. Cement and Concrete Research, 2018. **108**: p. 152-166.
29. Costa, A. and J. Appleton, Chloride penetration into concrete in marine environment—Part I: Main parameters affecting chloride penetration. Materials and Structures, 1999. **32**(4): p. 252.
30. Collepardi, M., A. Marcialis, and R. Turriziani, Penetration of chloride ions into cement pastes and concretes. Journal of the American Ceramic Society, 1972. **55**(10): p. 534-535.
31. Cai, H. and X. Liu, Freeze-thaw durability of concrete: ice formation process in pores. Cement and Concrete Research, 1998. **28**(9): p. 1281-1287.
32. Molero, M., et al., Evaluation of freeze–thaw damage in concrete by ultrasonic imaging. NDT & E International, 2012. **52**: p. 86-94.
33. Sun, J. and L. Lu, Coupled effect of axially distributed load and carbonization on permeability of concrete. Construction and Building Materials, 2015. **79**: p. 9-13.
34. Bao, J. and L. Wang, Combined effect of water and sustained compressive loading on chloride penetration into concrete. Construction and Building Materials, 2017. **156**: p. 708-718.
35. Sun, W., et al., Damage and damage resistance of high strength concrete under the action of load and freeze-thaw cycles. Cement and Concrete Research, 1999. **29**(9): p. 1519-1523.
36. Tsivilis, S., et al., A study on the parameters affecting the properties of Portland limestone cements. Cement and Concrete Composites, 1999. **21**(2): p. 107-116.

37. Standard, C., GB/T, 50081-2002 Method for testing mechanical properties of normal concrete. Beijing, China, 2002.
38. Lu, W., et al., Influence of an applied compressive load on capillary absorption of concrete: observation of anisotropy. Restoration of Buildings and Monuments, 2014. **20**(2): p. 131-136.
39. Standard, C.I., Testing methods for long-term and long-lasting performance of ordinary concrete, Construction Industry Publications;GB/T 50082-2009. 2009, Standard Press of China: Beijing, China.
40. Pigeon, M., R. Pleau, and P.-C. Aitcin, Freeze-thaw durability of concrete with and without silica fume in ASTM C 666 (Procedure A) test method: internal cracking versus scaling. Cement, concrete and aggregates, 1986. **8**(2): p. 76-85.
41. Wittmann, F., et al. Service life of reinforced concrete structures under combined mechanical and environmental loads. in 2nd International Symposium on Service Life Design for Infrastructures. 2010. RILEM Publications SARL.
42. Hall, C., Water movement in porous building materials—I. Unsaturated flow theory and its applications. Building and Environment, 1977. **12**(2): p. 117-125.
43. Litvan, G.G., Phase transitions of adsorbates. V. Aqueous sodium chloride solutions adsorbed of porous silica glass. Journal of Colloid and Interface Science, 1973. **45**(1): p. 154-169.
44. Castro, J., D. Bentz, and J. Weiss, Effect of sample conditioning on the water absorption of concrete. Cement and Concrete Composites, 2011. **33**(8): p. 805-813.
45. Hong, F. and Z. Tiejun, DRB-H1 Fourth Generation Concrete Grinding Machine, in Patent, China. 2004.
46. Zhang, Q., et al., Diffusion kinetics of sodium chloride in Grass carp muscle and its diffusion anisotropy. Journal of Food Engineering, 2011. **107**(3): p. 311-318.
47. LI, S. and W. SUN, Review on deterioration of concrete subjected to coupling effect of fatigue load, carbonation and chlorides. Journal of The Chinese Ceramic Society, 2013. **41**(11): p. 1459-1464.
48. Wang, H., et al., Effect of External Loads on Chloride Transport in Concrete. Journal of Materials in Civil Engineering, 2011. **23**(7): p. 1043-1049.
49. Shang, H.-s. and Y.-p. Song, Behavior of air-entrained concrete under the compression with constant confined stress after freeze–thaw cycles. Cement and Concrete Composites, 2008. **30**(9): p. 854-860.
50. Wittmann, F., P. Zhang, and T. Zhao, Influence of combined environmental loads on durability of reinforced concrete structures. Restoration of Buildings and Monuments, 2006. **12**(4): p. 349-362.
51. Zhang, P., et al., Self-healing behaviour of multiple microcracks of strain hardening cementitious composites (SHCC). Construction and Building Materials, 2018. **169**: p. 705-715.
52. Dry, C., Three designs for the internal release of sealants, adhesives, and waterproofing chemicals into concrete to reduce permeability. Cement and Concrete Research, 2000. **30**(12): p. 1969-1977.
53. Qi, C., J. Weiss, and J. Olek, Characterization of plastic shrinkage cracking in fiber reinforced concrete using image analysis and a modified Weibull function. Materials and Structures, 2003. **36**(6): p. 386-395.

54. Matallah, M., C. La Borderie, and O. Maurel, A practical method to estimate crack openings in concrete structures. International Journal for Numerical and Analytical Methods in Geomechanics, 2010. **34**(15): p. 1615-1633.
55. Samaha, H.R. and K.C. Hover, Influence of microcracking on the mass transport properties of concrete. Materials Journal, 1992. **89**(4): p. 416-424.
56. Wang, K., et al., Permeability study of cracked concrete. Cement and concrete research, 1997. **27**(3): p. 381-393.
57. Jiang, W.-q., et al., A numerical study on chloride diffusion in freeze-thaw affected concrete. Construction and Building Materials, 2018. **179**: p. 553-565.
58. Osio-Norgaard, J., J.P. Gevaudan, and W.V. Srubar, A review of chloride transport in alkali-activated cement paste, mortar, and concrete. Construction and Building Materials, 2018. **186**: p. 191-206.
59. Wittmann, F.H., et al. Influence of an imposed tensile stress and subsequent self-healing on capillary absorption and chloride penetration into HPFRCC. in High Performance Fiber Reinforced Cement Composites. Stuttgart: International RILEM Workshop. 2015.

545 Table 1 Chemical compositions of Portland cement used in this study

Raw materials	Components (mass% as oxide)										
	CaO	SiO_2	Al_2O_3	MgO	SO_3	Fe_2O_3	K_2O	TiO_2	MnO	Na_2O	P_2O_5
P.I. 52.5	57.27	20.60	7.17	4.70	4.43	3.85	0.77	0.40	0.35	0.17	0.13

546

547

548 Table 2 Mix composition of concrete

Concrete	Water/Cement	Cement (kg/m^3)	Sand (kg/m^3)	Aggregate (kg/m^3)	Water (kg/m^3)	Superplasticizer
C30	0.53	375	750	1125	200	/
C50	0.35	450	675	1125	156.1	2.0%

549

550 Table 3 Result of ultimate compression test

Concrete	Slump (mm)	Air content (%)	Bulk density (kg/m^3)	f_c (MPa)	0.3f_c (MPa)	0.5f_c (MPa)
C30	50	3.7	2414	38.47	12.2	20.3
C50	60	2.4	2470	54.95	17.4	28.9

551 f_c, the ultimate compressive strength after 28d curing, MPa

552

553 Table 4 Definition of different specimens

Specimen	Compressive stress /f_c	Freezing-thawing cycles /cycle	Part
0-0-i	0f_c	0	Inside
0-0-o	0f_c	0	Outside
0-25-i	0f_c	25	Inside
0-25-o	0f_c	25	Outside
30-25-i	0.3f_c	25	Inside
30-25-o	0.3f_c	25	Outside
50-50-i	0.5f_c	50	Inside
50-50-o	0.5f_c	50	Outside

554

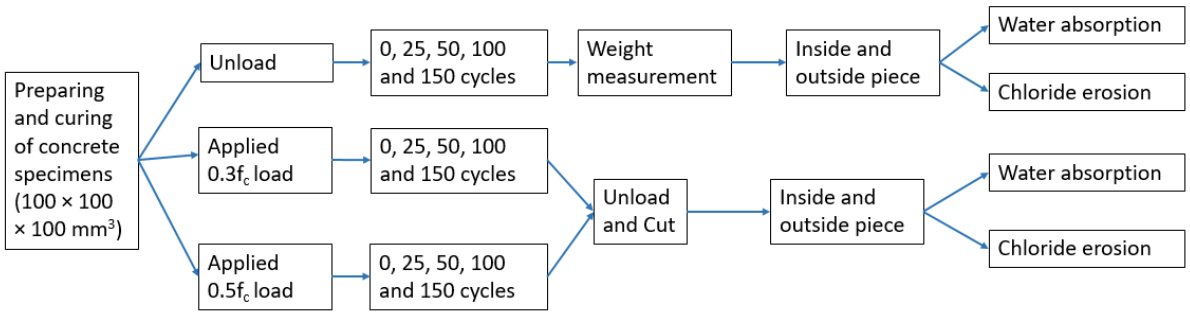

555

556 Fig. 1. Sequence of test flow

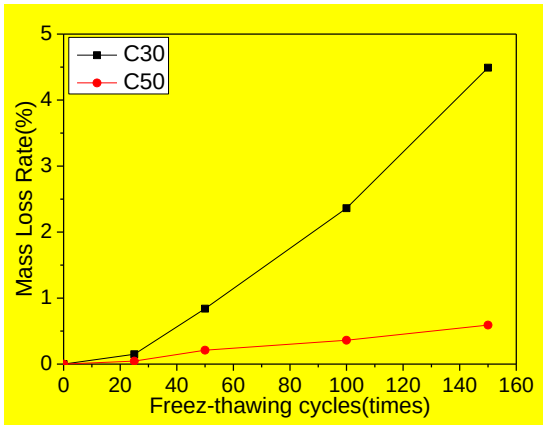

Fig. 2. The mass loss of concrete

560 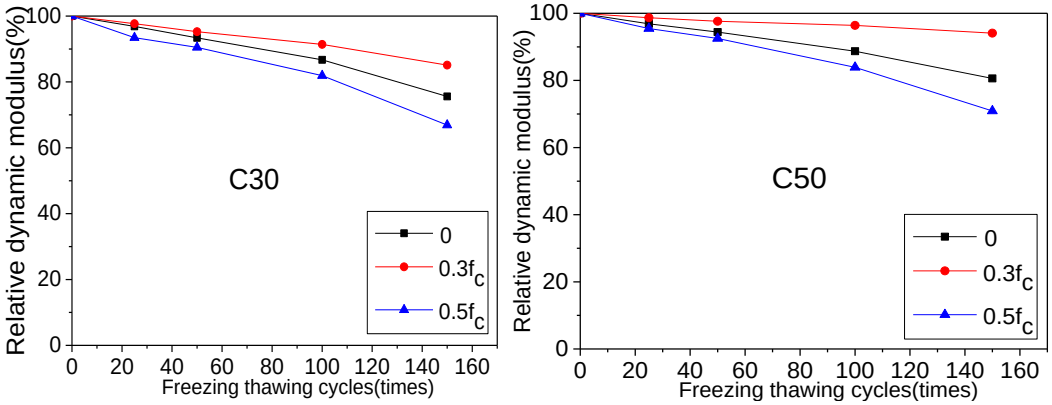

561 Fig. 3. The relative dynamic modulus (RDM) of C30 and C50 with the coupling effect of
562 frost cycles and load

563

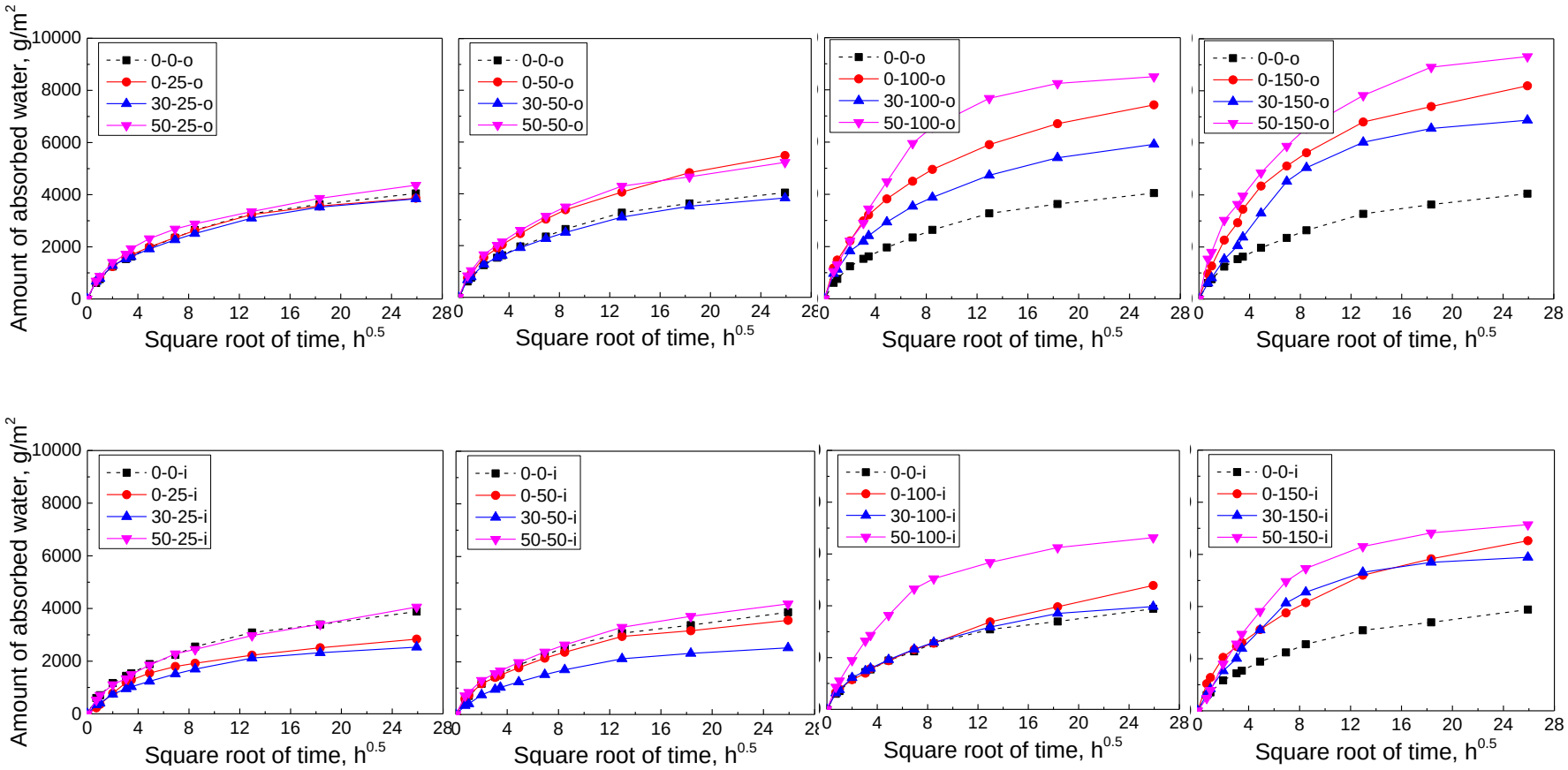

Fig. 4. Amount of absorbed water of C30 with the coupling effect of frost cycles and load

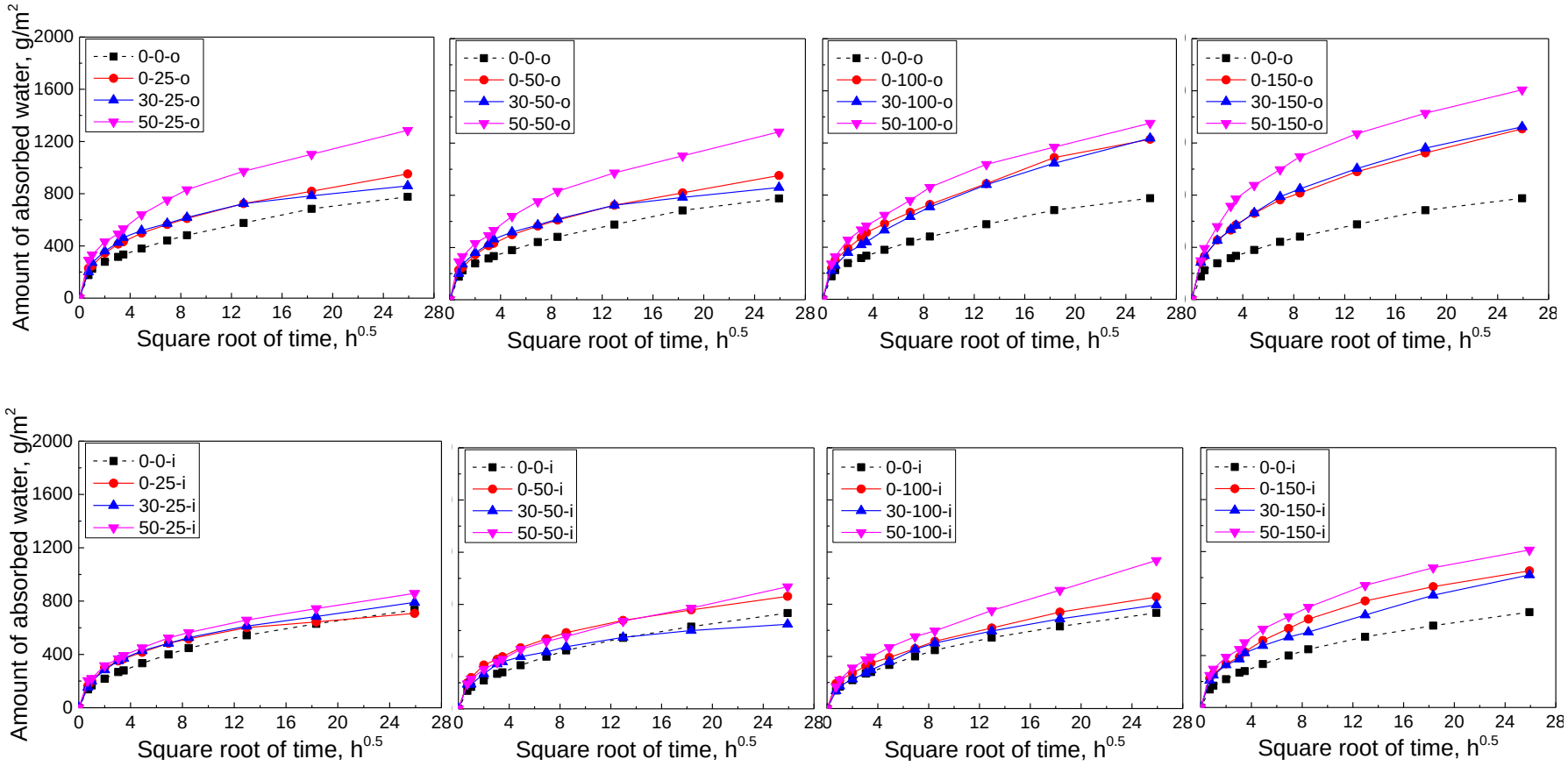

Fig. 5. Amount of absorbed water of C50 with the coupling effect of frost cycles and load

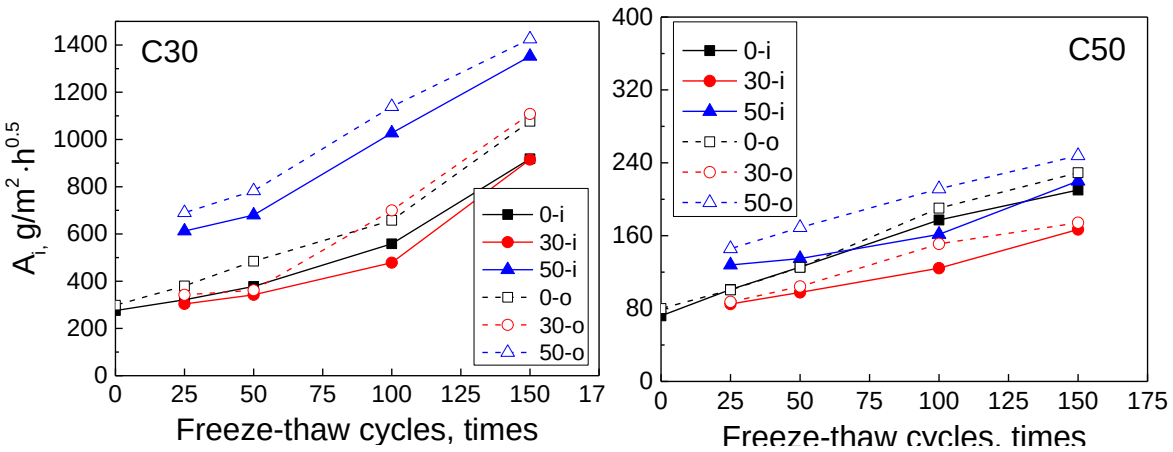

Fig. 6. Initial water absorption coefficient of C30 and C50 as function of freeze-thaw cycles

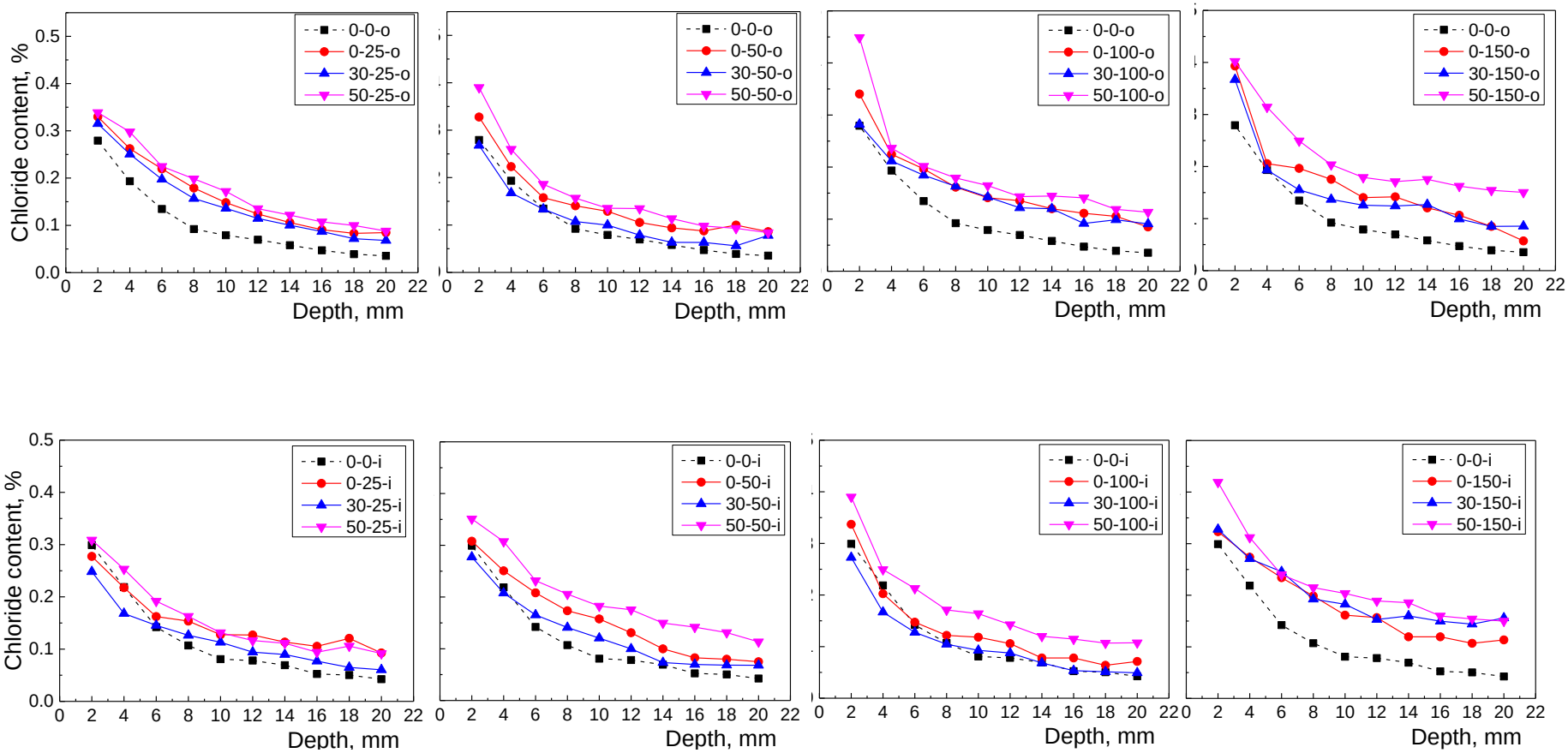

Fig. 7. Chloride ion content of C30 concrete after 7d chloride penetration

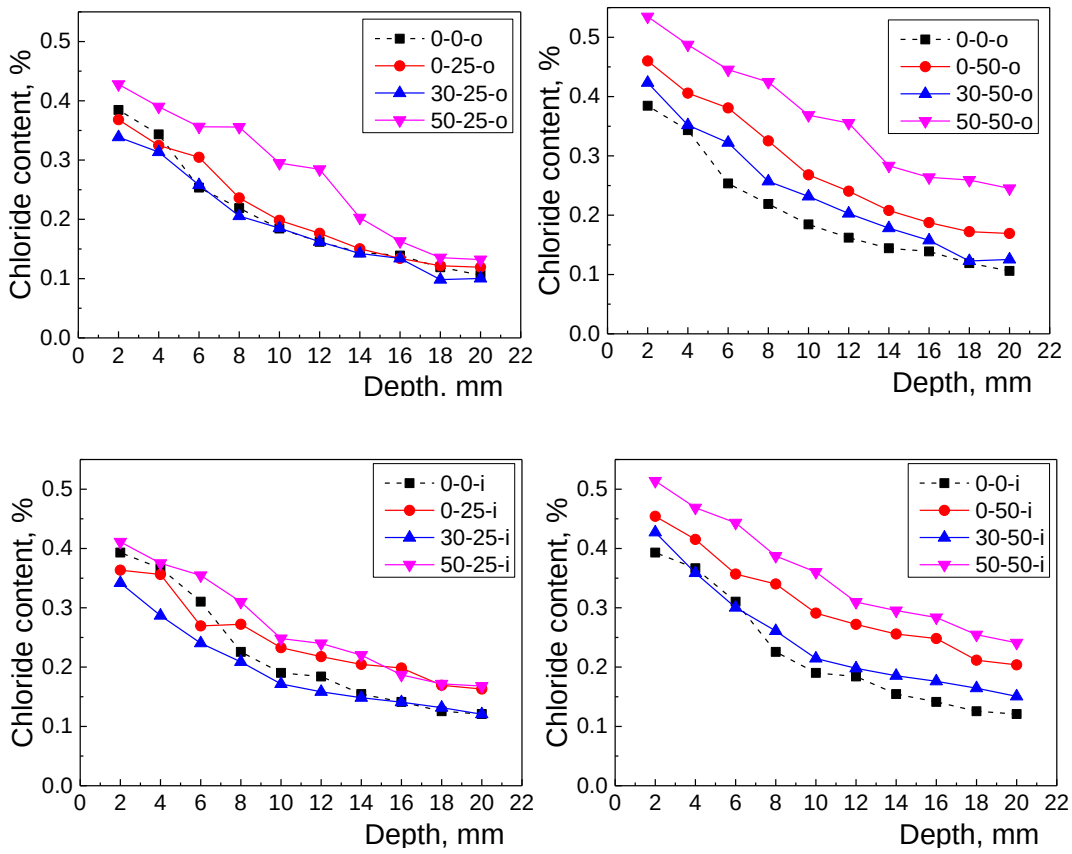

Fig. 8. Chloride ion content of C30 concrete after 28d chloride penetration

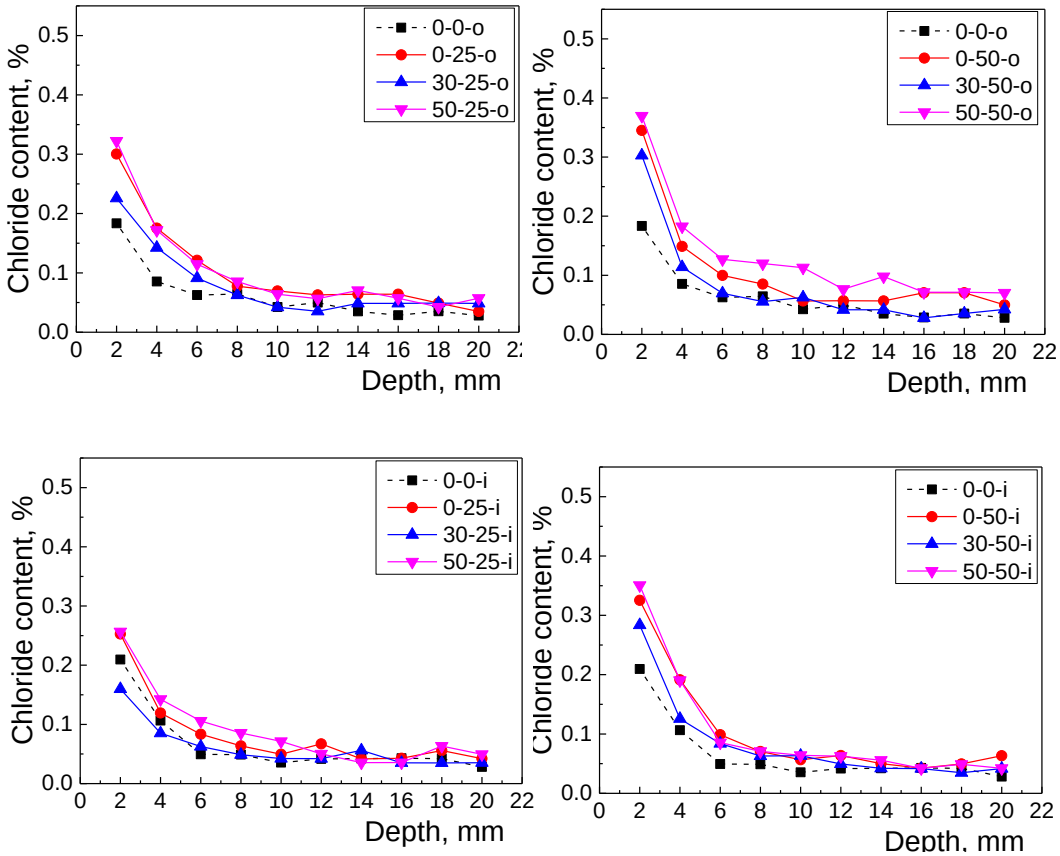

Fig. 9. Chloride ion content of C50 concrete after 7d chloride penetration

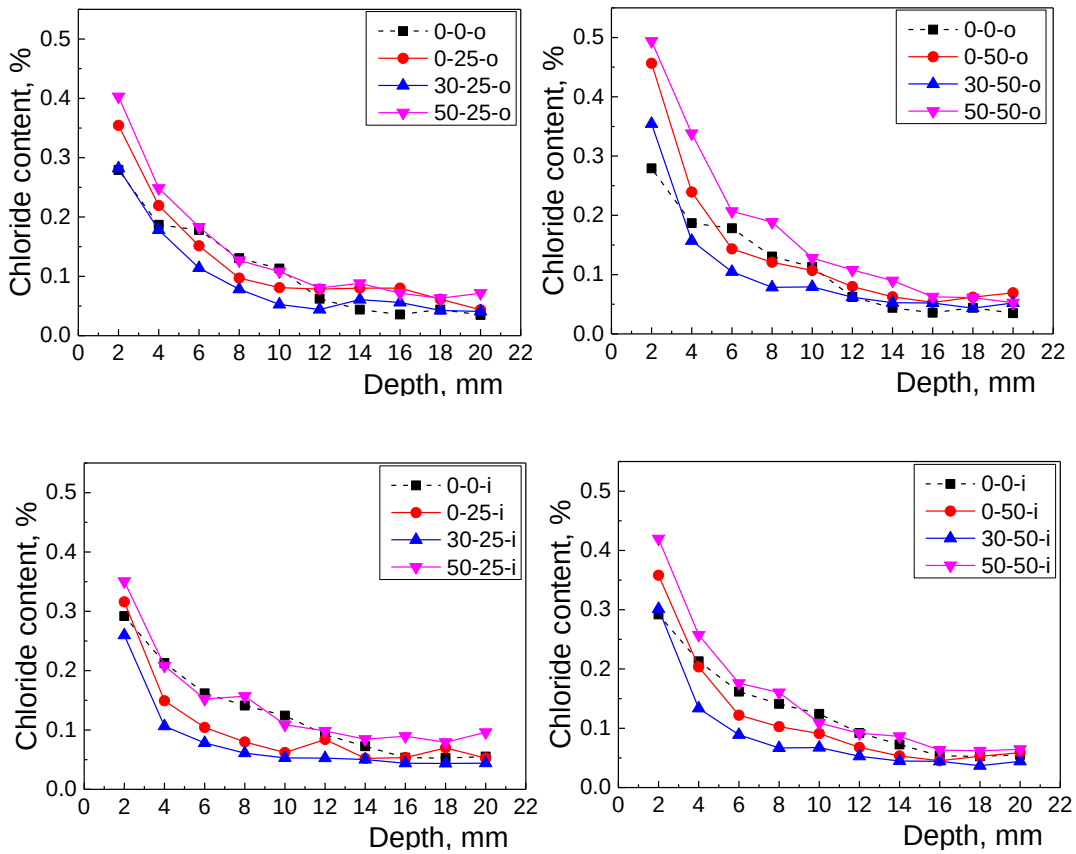

Fig. 10. Chloride ion content of C50 concrete after 28d chloride penetration

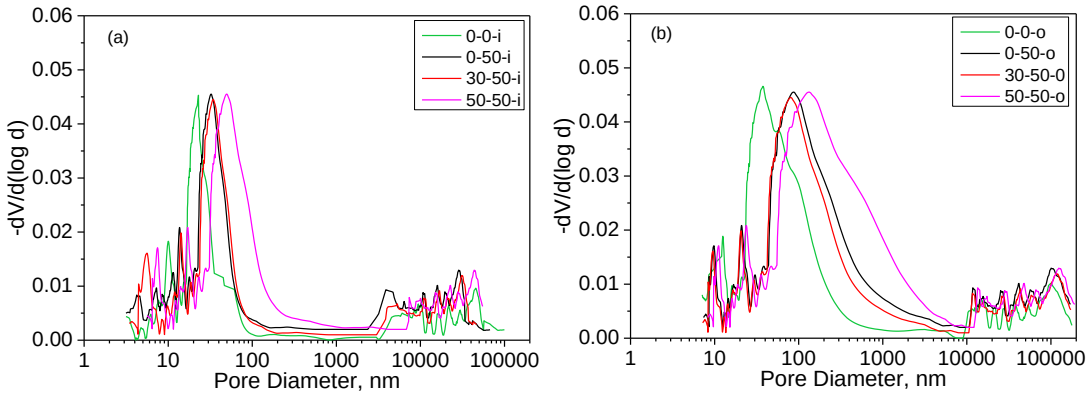

12

13 Fig. 11. Pore size distribution of C30 concrete under compiling effect